Colloids and Surfaces B: Biointerfaces 247 (2025) 114422

Contents lists available at ScienceDirect

Colloids and Surfaces B: Biointerfaces

journal homepage: www.elsevier.com/locate/colsurfb

Curious effects of overlooked aspects on urease activity

Mert Acar [a], Duccio Tatini [b], Valentina Romani [a], Barry W. Ninham [c], Federico Rossi [d], Pierandrea Lo Nostro [a,*]

[a] Department of Chemistry "Ugo Schiff" and CSGI, University of Florence, Sesto Fiorentino, Firenze 50019, Italy
[b] Department of Biotechnologies, Chemistry and Pharmacy, University of Siena, Siena 53100, Italy
[c] Department of Materials Physics, Research School of Physics, Australian National University, Canberra, ACT 0200, Australia
[d] Department of Earth, Environmental and Physical Sciences-DEEP Sciences, University of Siena, Siena 53100, Italy

ARTICLE INFO

Keywords:
Hofmeister series
Kosmotropicity
Chaotropicity
Dissolved gases
Heavy water
Enzymatic activity
Urease

ABSTRACT

Intermolecular forces determine complex chemical structures of exquisite intricacy, like proteins. However even the most advanced theories we have so far rely on too drastic approximations to explain them. Some crucial aspects that dictate structure, specific ion and solvent effects are not accommodated. Further the very significant effects of dissolved atmospheric gas are completely ignored and unexplored. Here we examine the effects of cations, dissolved gasses, and heavy water on the pH clock reactions of urease. This enzyme catalyzes the hydrolysis of urea to ammonium and bicarbonate in unbuffered aqueous solutions. In so doing it increases the pH. Circular dichroism and fluorescence experiments are used to assess conformational effects. The results highlight the subtle interplay of different factors that participate in determining the urease activity. The experimental data are correlated with specific ion physicochemical parameters and conformational data. They are explored in the context of specific ion and solvent interactions and hydration.

1. Introduction

Biological organisms represent one of the most intricate designs of biomaterials and apparently are the masterpiece of evolution. Proteins and enzymes are the central actors in the processes of life. Intermolecular forces are imperative in these designs and constitute the main building blocks of the most complex chemical architectures. However, these forces are multifaceted, and some of their aspects, such as specific ion and solvent effects, micro- and nanobubbles, remain mostly unexplored. These *'hidden iceberg'* features of solvents and electrolytes represent gaps in our knowledge and can exert a remarkable influence on various mechanisms, leading to unexpected anomalous behaviors. For example, some salts can stabilize proteins or enhance the activity of enzymes, while other induce salting out and denaturation in proteins. The mechanism through which ions affect the physical chemistry of their simple solutions and of the more complex systems in which they are found (e.g., formulations, body fluids, natural environments) is still an attractive and unresolved object of investigation.

Urease, an enzyme from the superfamily of amidohydrolases and phosphotriesterases, catalyzes the hydrolysis of urea to form ammonium and bicarbonate ions. This results in a pH increase in unbuffered aqueous solutions. (Scheme 1) [1].

The urease/urea reaction follows Michaelis-Menten kinetics and has a bell-shaped pH-rate curve. The peak activity is around pH 7 [2]. When the reaction is initiated under acidic conditions, an increase in pH accelerates the reaction up to pH 7. However, a further increase in pH leads to a strong inhibition of the enzyme activity. This results in a sigmoidal pH *vs.* time reaction curve [2–4]. Thus, by adjusting the initial pH of the solution, one can induce a clock-type reaction, leveraging the pH-dependent nature of enzyme activity [1–5].

Urease is a common enzyme found in bacteria, microorganisms, plants, and soil [6]. For instance *Helicobacter pylori*, a urease containing bacterium, is implicated in chronic gastritis, ulcers and even gastric cancer [7,8]. Although the search for biocompatible inhibitors of urease is imperative from a biomedical perspective [6,7], its potential extends far beyond. Some examples of urease use in applicative sciences include the development of chronoresponsive materials [3,9], the design of soft actuators [10–13], microrobots, and microswimmers [14–17], the creation of artificial enzymatic networks [18], reaction-diffusion mediated patterned coatings [19], pH gradients in microenvironments [20,21] and pH oscillators [2,22–24].

Here we explore how the urease catalyzed hydrolysis of urea

* Corresponding author.
E-mail address: pierandrea.lonostro@unifi.it (P. Lo Nostro).

https://doi.org/10.1016/j.colsurfb.2024.114422
Received 29 June 2024; Received in revised form 15 November 2024; Accepted 2 December 2024
Available online 6 December 2024

responds to variations of the solution environment. In particular we consider in succession:

Ions. Ions are key players everywhere, e.g. in oleate-based wormlike nanostructures where Na^+ and K^+ compete for interfacial binding and determine the size and morphology of the aggregate [25] and in cell biology where the content of cations inside and outside the cell cytoplasm is highly asymmetric [26]. Classical theories for the electrolyte solutions, e.g. for the calculation of ionic activity coefficients and of pH and buffers, are impotent at biological salt concentrations of effectively 0.14 M [27]. At and above this concentration theory fails and ion specificity emerges. One reason is that it can be shown that dispersion forces between ions become larger than electrostatic forces. And dispersion forces are omitted from theory [28].

Some aspects of specific ion effects are frequently oversimplified. For instance, the weaker effect attributed to cations compared to anions, and the additivity of the effects induced by cations and anions [27].

Deuterium. In the same vein solute-solvent interactions can profoundly change the overall narrative. For example, D_2O is present in ordinary water at 157 ppm [29]. Variation of D_2O content can provide new insights into molecular behavior in aqueous solution or dispersion, like the nature of hydrogen bonding [30].

Dissolved Gas. Water has almost invariably been treated theoretically as a molecular liquid. Such a conceptualization cannot explain manifestations of its complex structure in Nature. So, for example, the presence of dissolved gases is completely ignored in theory and in simulations, however gas is essential to metabolism in both aquatic and land life. Oxygen and nitrogen are taken up by organized lung surfactant and delivered to the capillaries as nanobubbles, stable above physiological salt concentration [31].

Salt solutions exhibit the phenomenon of bubble-bubble fusion inhibition above 0.17 M for some salts [32]. The same occurs for sugars [33] and for amino acids [34].

These phenomena cannot be explained by classical theories of physical chemistry. The phenomena point to the involvement of nanobubbles in the range about 3–5 nm with depletion forces imposing stability against fusion of macro bubbles. The most direct evidence is from measurements of conductivity of electrolytes in ordinary and degassed conditions [35].

More recently the amount of atmospheric gases dissolved in the deep Northern Atlantic waters disclosed interesting effects on the marine nitrogen cycle and its role in ocean carbon storage [36]. The drastic depletion of gases from solutions with freeze-and-thaw procedures leads to convincing demonstration of the paramount importance of dissolved gases in liquids. Similarly, effects for cloud point of a short chain phospholipid [37], the formation of polypseudorotaxanes [38], the spectral properties of dyes [39], and the phase separation of immiscible liquids [35].

In a previous paper we have already shown the effect of different anions on the activity of urease [40]. Here we report on the effects of cations (with fixed anion), dissolved gasses, and D_2O on the pH-clock reactions of urease in unbuffered aqueous solutions. In particular we studied LiCl, NaCl, KCl, CsCl, $MgCl_2$, $CaCl_2$ and $BaCl_2$. Circular dichroism and fluorescence experiments were used to further elucidate the conformational role in these complex mechanisms.

Now the questions are: how do cations affect the activity of urease and what is the role of deuterium replacement and of the dissolved gasses in modifying the performance of urease at room temperature? That is that this work is about.

2. Materials and methods

2.1. Chemicals

Milli-Q water from Millipore with a resistivity of 18.2 MΩ•cm and a conductivity of 0.055 μS•cm^{-1} was used. The following salts were used in experiments: LiCl, NaCl, KCl, CsCl, $MgCl_2$•6 H_2O, $CaCl_2$•2 H_2O, $BaCl_2$•2 H_2O. The salts (≥99 %), D_2O (99.9 atom % D), HEPES (≥99.5 %) and urea (99.5 %) were purchased from Merck (Milan, Italy). Urease (from Jack Bean, min. 300 unit/mg) was purchased from TCI-Europe N.V. (Zwijndrecht, Belgium). CH_3COOH (≥99.7 %) and H_2SO_4 (98 %) were purchased from Merck (Milan, Italy) and used to adjust the initial pH of the solutions. All stock solutions of urease, urea, and salts were freshly prepared.

The definition of a urease unit was taken as 1.0 μmol of NH_3 liberated from urea per minute at pH 7.0 and 25° C. The enzymatic activity was determined using an ammonium ion-selective electrode ISE NH_4^+ 9663 C purchased from Hach (Lainate, Italy), using the procedure described in detail in ref. [40].

2.2. Removal of dissolved gases

Solutions were degassed by *Freeze and Thaw* (FPT) procedure. The vacuum system (Figure S1 in Supplementary Materials) comprises an oil rotary pump with two stage vanes, model RV 25D (Arcatec srl, Cologno Monzese, Italy). Through a Rotulex 19/9 junction, a high vacuum tube (Disa, Milano, Italy) is connected to the pump. Between the tube and the pump, a liquid nitrogen trap is located in order to block the water vapor from entering the pump. The pump nominal rate is 5.4 m^3/h with a final pressure of 2 mbar and a motor power of 0.12 kW.

The degassed solutions (urea and H_2SO_4 in water) were prepared with reaction volumes similar to those of the blank. The enzyme was added only after degassing had already been carried out, as the enzyme is susceptible to thermal shock. Three degassing cycles were performed. First, the solution is introduced into a Pyrex tube and subjected to freezing in liquid nitrogen within a Dewar flask for a minimum duration of 15 minutes. Then, the vacuum valve is opened to facilitate the removal of gases through fissures in the ice. This procedure operates optimally within a pressure range of 10^{-4} to 10^{-7} atm and persists for 90 minutes, after which the vacuum valve is closed again. In the final step, the sample is brought back to ambient temperature and pressure. For the experiments on readmission, the degassed solutions were bubbled with the gas of interest for 30 mins at room temperature. For the readmission of air the sample was left in the open test tube for either 1 hour or 6 hours before repeating the experiment.

2.3. pH measurements

The enzymatic reaction was investigated by pH measurements over time, initially in the presence of salts. They were followed by experiments in heavy water at various concentrations, and finally in degassed solutions, all under non-buffered conditions. All reactions were performed under magnetic stirring and thermostat at 25 °C. A fixed incubation time of 10 seconds was imposed for urease and salts before starting the reaction. pH measurements were made by using an XS pHsensor 201 T DHS (Carpi, Italy) and Amel pHmeter 2335 (Milan, Italy) by recording values every second. To estimate the speed of the process, the derivatives of the pH value (∂pH/∂t) as a function of time were calculated for each curve.

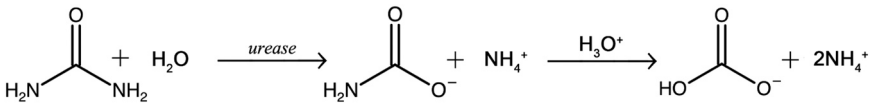

Scheme 1. Urease-catalyzed hydrolysis of urea into ammonium and hydrogen carbonate ions.

The kinetic profile is dependent on the activity of urease solutions. Some examples in this regard can be found in Fig. 1, panel a. Analyzing the pH rate over time (∂pH/∂t), we observe two main maximum peaks corresponding to the enzymatic reaction, with both contributions distinctly visible at low enzymatic activity (<1 U/mL). The time it takes for the reaction to reach the second maximum peak is assigned as the *clock time* (Fig. 1, panel b). To obtain the sigmoidal behavior, an initial acidic pH is required.

The experimental clock times (t_c) and the maximum of the first derivative in the pH *vs.* time curve were normalized to the blank, and gave the two benchmark parameters, τ and δ respectively. These are defined by Eqs. 1 and 2:

$$\tau = \frac{t_{c,solution} - t_{c,blank}}{t_{c,blank}} \quad (1)$$

$$\delta = \frac{\max\left(\frac{\partial pH}{\partial t}\right)_{solution} - \max\left(\frac{\partial pH}{\partial t}\right)_{blank}}{\max\left(\frac{\partial pH}{\partial t}\right)_{blank}} \quad (2)$$

Here $t_{c,blank}$ and $t_{c,solution}$ are the clock time for the blank and for the solution, respectively. The maxima of the first derivative ∂pH/∂t were used.

Cation Effects. The reference system for electrolyte study comprised 10 mM urea and 5 U/mL urease, as in our previous study on the effects of anions [40]. The initial pH was set to 3.6 by adding the necessary amount of CH_3COOH. Under these conditions, the reference clock time was approximately 180 s, and the final pH was around 9.

Specific ion effects result in changes in the measured pH [41]. The addition of cations induces a dependence of pH on the added salts. To ensure that there were no artifacts in the final results caused by such pH changes, we evaluated changes in the clock time and maximum velocity by altering the initial pH value. We then were able to confirm that the observed effects could be attributed to the different added ions.

Solvent Effects. The reference system consisted of 0.5 U/mL urease for studies involving heavy water and degassed solutions. The initial pH was set to 3.6 by adding the necessary amount of H_2SO_4. Under these conditions, the reference clock time was approximately 180 s, with a final pH around 9.2.

2.4. Fluorescence spectroscopy

Fluorescence measurements were performed at 25 °C using an LS50B Perkin Elmer spectrofluorimeter equipped with a Haake thermostat. Samples were prepared in 1 cm optical path-length quartz cuvettes from Hellma (Muellheim, Germany). Experiments were carried out with 0.08 mg.mL^{-1} urease aqueous solutions in the presence of salts. The tryptophan (*Trp*) fluorescence was monitored for conformational changes. Emission spectra were recorded with a 100 nm.min^{-1} scan speed in the 320–450 nm range using 295 nm excitation wavelength with 10 x 5 nm width of slits for excitation and emission, respectively. Each spectrum was accumulated from 5 spectra. At each salt concentration, a blank spectrum consisting of water and salt was recorded, and the spectra was subtracted as background.

2.5. Circular dichroism

CD spectra were recorded using a J-715 Jasco spectropolarimeter with a 200 nm.min^{-1} scan speed and data points were collected from 200 to 280 nm at 25° C with a 1 mm Hellma quartz cuvettes from Hellma (Muellheim, Germany). Experiments were carried out in 0.5 mg.mL^{-1} urease aqueous solutions in the presence of salts. Each spectrum was accumulated from 5 spectra and the blank signal acquired for the water was subtracted.

2.6. ζ-Potential

The ζ-potential was measured with a Brookhaven Instruments 90 Plus (Brookhaven, Holtsville, NY) and calculated from electrophoretic mobility (μ) using the Helmholtz–Smoluchowski equation ($\zeta = \mu \cdot \eta/\varepsilon$), where η is the viscosity and ε is the dielectric permittivity of the medium. Each value is the average of 10 measurements.

3. Results and discussion

3.1. Specific cation effects

The values of τ and δ (see Eqs. 1 and 2) were calculated at different salt concentrations and are listed in Tables S1 and S2 (see the Supplementary Material). An inhibitory effect of all salt solutions was observed. There was, typically, an increase in τ and a decrease in δ.

The trend for both τ and δ at 0.02 M is:

$$Cs^+, K^+ < Na^+ < Ba^{2+} \sim Li^+, Mg^{2+} < Ca^{2+}$$

In some cases, the position of divalent cations in the Hofmeister series strongly depends on the system under investigation [42]. For example, in albumin precipitation the ranking of divalent cations is $Mg^{2+} > Ca^{2+} > Ba^{2+}$, while the lyotropic series shows a different trend [43,44].

Fig. 2, panel a, shows the τ values *vs.* concentration for all cations. The monovalent ions Na^+, K^+, and Cs^+ have very similar trends, while Li^+ shows a different behavior. Na^+ has the least effect on the clock time. It deviates from the trend of K^+ and Cs^+ only at high concentrations, (above 70 mM). This behavior spots Na^+ as the most tolerated ion, in

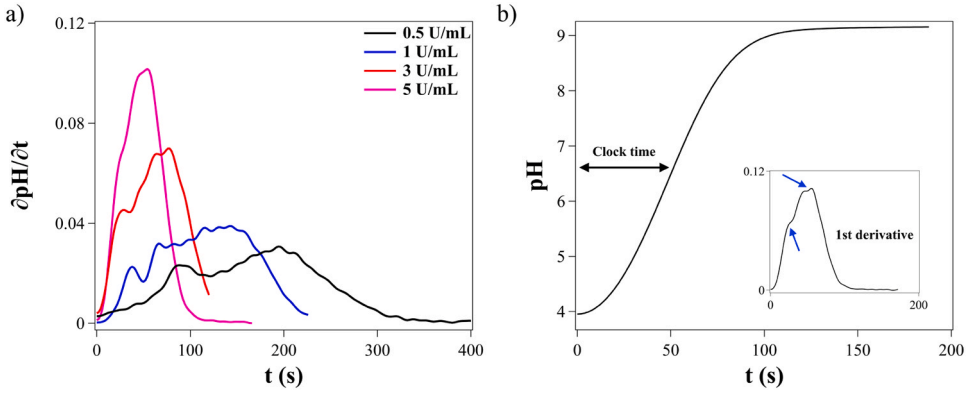

Fig. 1. (a) *∂pH/∂t vs. t* at different urease concentrations in salt free samples. (b) Variation of pH *vs. t*. The clock time (t_c) is the time elapsed between the start of the reaction and the point of inflection. Inset: *∂pH/∂t vs. t* from the same dataset. The blue arrows point at the two maximum peaks. The time necessary for the reaction to reach the second maximum corresponds to the clock time.

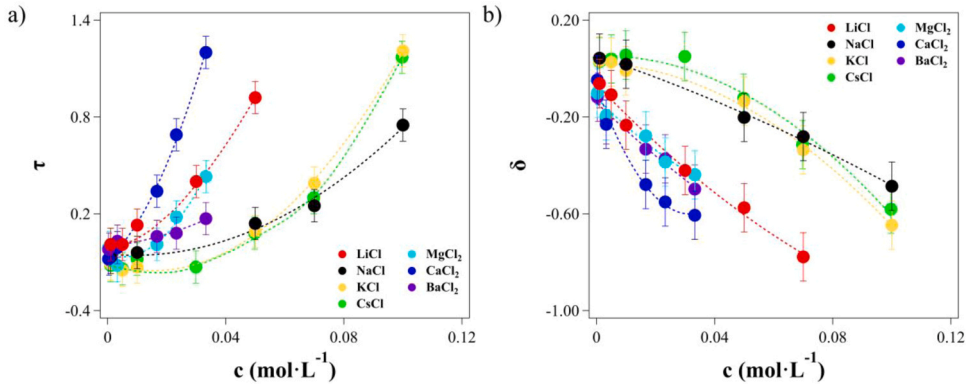

Fig. 2. (a) τ and (b) δ values for the cation series at increasing concentrations of salts at 25° C. The dotted lines are guides for the eye.

passing we recall that Na^+ like Cl^- marks the midpoint between kosmotropes and chaotropes [40]. In fact, all biomolecules and life evolved on Earth in the presence of large amounts of NaCl [45–47], as it is present in seawater (3.5 wt%) [48], in underground rock formations, as the mineral halite and as mixed evaporites in salt lakes [49]. These are probably the reasons for the great tolerance of enzymes toward sodium chloride.

On the other hand, the presence of Li^+ leads to a significant inhibition of the enzyme already at low salt concentrations (about 10 mM).

In the case of divalent cations, we observe a curious trend. The addition of Ca^{2+} results in a τ/c curve that dominates all those with other cations. Magnesium has a similar effect to that of Li^+, maybe related to the small size and high charge density of the two cations, that largely contribute to their large hydration Gibbs free energies (-475 for Li^+ and −1830 kJ/mol for Mg^{2+}) [50]. Ba^{2+}, on the other hand, seems to have a mild effect on the clock time.

In general the addition of a salt decreases the maximum velocity of the reaction and the values of δ. Fig. 2, panel b, shows the δ/c plot for the investigated electrolytes. We remark that Li^+ is the only monovalent cation that follows a different behavior respect to the other alkaline ions, in fact its trend looks very similar to that of divalent alkaline earth cations. Na^+, K^+ and Cs^+ induce different effects depending on the salt concentration. At very low concentration, below 30 mM, δ is similar to the value in pure water, and the trend is $Na^+ \leq K^+ < Cs^+$. For higher concentrations δ decreases significantly and above 80 mM the trend is reversed: $Na^+ > K^+ > Cs^+$.

The δ values for $MgCl_2$ and $BaCl_2$ overlap, while their τ values were very well separated. In other words, the process is accelerated in the early steps of hydrolysis, i.e. for pH < 7 producing slight changes in the clock time. The plot also shows that while Mg^{2+} and Ba^{2+} behave like Li^+, Ca^{2+} has a stronger effect on the maximum rate of the enzymatic reaction. Moreover, whereas the addition of Ba^{2+} induces only slight changes in the clock time and remarkable changes in the maximum rate, Mg^{2+} and Ca^{2+} mirror the behavior of their τ values.

To elucidate this effect, we plotted *∂pH/∂t vs. t* in the presence of different salts at 0.1 M ionic strength (Fig. 3). Firstly we observed a third local maximum in the reaction rate, most likely due to a splitting in the second local maximum.

While the first rate maximum remains constant over time, the second and third maxima shift depending on the composition of the added salt. For Li^+, K^+, Cs^+, and Ca^{2+}, similar patterns of inhibition and shift are observed. Instead, Mg^{2+} and Ba^{2+} exhibit markedly different behaviors, with an initial acceleration of the reaction rate as indicated by the first two red arrows in Fig. 3. This causes the third maximum, which determines the clock time, to occur at the same time as in the blank, despite a decrease in rate. This explains the differences recorded for δ and τ.

Notably also, Na^+ behaves differently, falling in between. This was expected, as at high concentrations Na^+ has a milder effect compared to other ions, as previously mentioned.

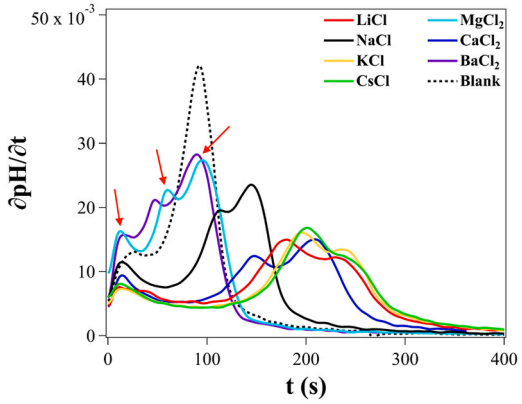

Fig. 3. The first derivative ∂pH/∂t *vs.* t for various salts at 0.1 M ionic strength. The dotted curve represents the salt free blank reaction. The red arrows indicate the local maxima in the reaction rate.

The origin of the local maxima in the urease enzymatic reaction rate is still unclear, and the results suggest that the mechanisms that govern the overall reaction are complex. We reasonably argue that hypothesis is that the enzyme may adopt different conformations at different pH values while the reaction proceeds, and these conformations are differently affected by the presence of co-solutes in the reaction medium.

3.1.1. *Interaction mechanism*

The urease active site comprises two Ni^{2+} ions bridged by a carbamylated lysine residue (see Figure S2 in Supplementary Materials). Each Ni^{2+} ion is coordinated by two histidine residues and a water molecule, with an additional bridge provided by a hydroxide ion. One Ni^{2+} ion adopts a pentacoordinated geometry, while the other has a hexacoordinated geometry due to an extra aspartate residue, resulting in a distorted octahedral arrangement [51]. The cavity of the active site is regulated by three water molecules, which form a tetrahedral cluster together with the hydroxyl group. Upon the entry of the urea substrate, the three water molecules leave the active site, and the enzyme-substrate interaction is made easier by a mobile flap that bears a crucial catalytic histidine residue [51].

In order to shed light on the interaction mechanism that controls the effect of cations on the enzyme activity we performed fluorescence and CD experiments. In each subunit, urease contains four residues of *Trp* [52]. Two of them, Trp^{648} and Trp^{708}, are deeply buried and stable. Instead, Trp^{728} is partially exposed, while Trp^{495} is exposed to the solvent [53]. These residues can provide some useful information on the interactions between the ionic species and the intrinsic fluorophores on the enzyme.

Fig. 4, panels a, b and c show the fluorescence spectra of salts at 0.1 M ionic strength. The characteristic features of the urease spectrum include a maximum peak at around 340 nm and a smaller shoulder at approximately 350 nm.

Trp fluorescence is exceptionally sensitive to solvent polarity, with a polar solvent inducing a red shift in the fluorescence emission. Burnstein *et al.* define three classes of *Trp* residues: *Trp* residues in a hydrophobic environment exhibits a fluorescence maximum around 330 nm (*Class I*), solvent exposed residues exhibit a value around 340 nm (*Class II*) and a value of 350 nm (*Class III*) is attributed to loose denatured coils in direct contact with the solvent [54]. However, it is important to recall that each protein exhibits a unique spectrum, and exceptions to these classes are possible. Indeed, the model assumes that the *Trp* residues are independent from one another and neglects the existence of energy transfer between tryptophyls within proteins [54].

Fig. 4, panel b, shows the deconvolution of the urease spectra using the Lognormal method [55]. The deconvolution parameters and the model values can be found in Table S3 (see the Supplementary Material). Notably $\Delta\lambda$ deviates from the expected Burstein model values [55]. This is particularly true in the case of the 330 nm peak ($\Delta\lambda$= 13 *vs.* 48–49 nm, respectively). Additionally, the contribution from this peak is minimal, despite the expectation that two deeply buried residues should contribute to it. It must be pointed out that the model relies on important assumptions, and there may also be an internal quenching mechanism that could account for the lack of a significant contribution. Indeed, previous findings reported in the literature show that deeply buried Trp^{648} and Trp^{708} residues provide almost no contribution to the fluorescence emission, in line with our findings [53].

The most significant contributions are the main 340 nm peak and the shoulder at 350 nm that likely correspond to partially solvent-exposed (Trp^{728} situated in the 33rd β-sheet) and fully solvent-exposed (Trp^{495} located in the tail of a β-turn domain) residues, respectively [53].

The addition of electrolytes does not appear to induce any changes to the environment of *Trp* residues. In all cases, various degrees of quenching are observed, as expected for ions in solution. Divalent cations are more efficient in fluorescence quenching with respect to monovalent species. However, there are no apparent shifts or shape changes in the peaks. This behavior is shown more clearly in Fig. 4, panel c, where the same spectra are presented on a normalized intensity scale for each salt.

Similarly, the CD measurements at 0.1 M ionic strength of these electrolytes show no ion-specific effect; they all show a moderately stronger secondary structure in all cases with respect to the electrolyte free samples (See Fig. 4, panel d).

The physicochemical parameters of ions can be used as descriptors to investigate correlations with the observed effects. In cases where one of the parameters has prominent effect, one can find a correlation with the

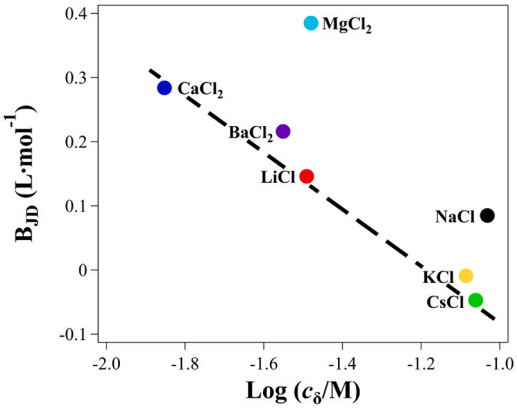

Fig. 5. Plot of the Jones-Dole *B* coefficient *vs.* Log(c_δ). Black dotted lines are guides for the eye and show the direct Hofmeister trend.

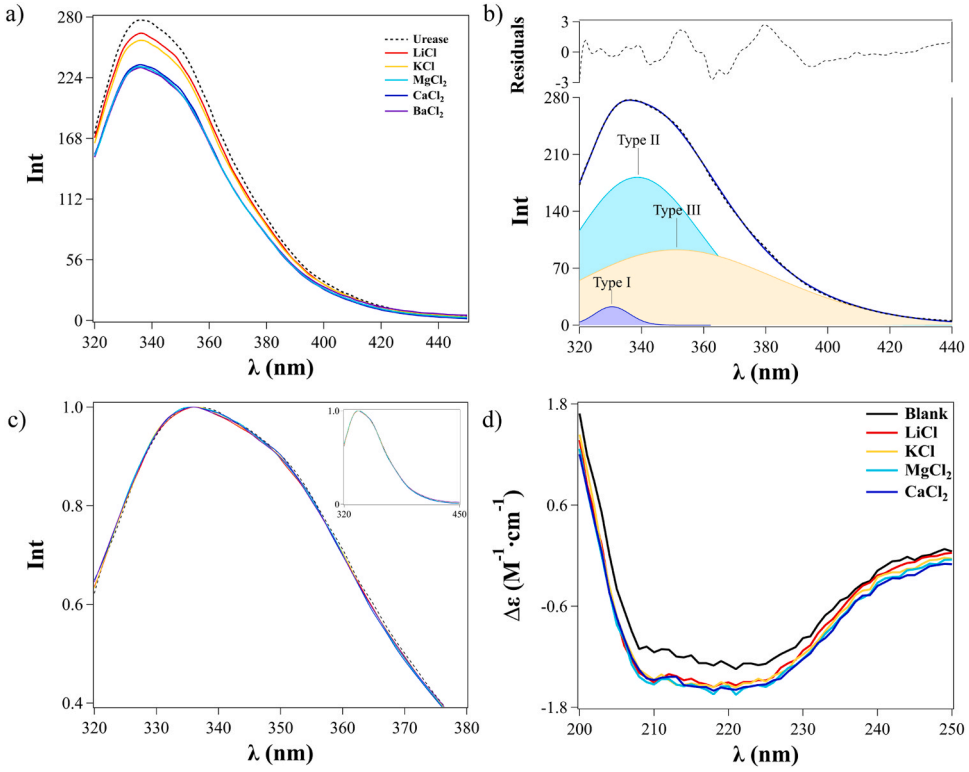

Fig. 4. (a) Urease *Trp* fluorescence spectra in the presence of LiCl, KCl, $MgCl_2$, $CaCl_2$ and $BaCl_2$ at 0.1 M ionic strength. The black dotted lines represent the salt-free samples. (b) Deconvolution of the urease fluorescence spectra with Lognormal fitting. (c) Each spectrum is represented in normalized intensity scale. The inset shows the entire range of the intensity profile. (d) Far-UV circular dichroism spectra of urease in the presence electrolytes at 0.1 M ionic strength.

observed trend.

Fig. 5 shows the concentration (in Log scale) needed to obtain a δ value of −0.5 for each salt as a function of the Jones-Dole B coefficients (B_{JD}). A linear correlation between the cation's B_{JD} coefficients and Log (c_δ) is observed. The B_{JD} coefficients, derived from the empirical Jones-Dole equation [56,57], reflect specific non-electrostatic solute-solvent interactions, such as van der Waals forces, hydration effects, hydrogen bonding, and dipole-dipole interactions, that emerge at moderate (*i.e.* non dilute) concentrations.

This correlation suggests that the dominating mechanism by which cations influence the enzymatic reaction is based on the solute-solvent intermolecular interactions. In our previous work we showed that the effects of anions, instead, depend on their interfacial properties and direct surface interactions with the enzyme [40].

Anions are in general more polarizable species; they possess more diffuse hydration shells and accumulate at interfaces more readily than cations [27]. These combined factors often result in anions having a greater effect on different systems compared to cations [27]. However, this does not exclude the possibility of indirect, *i.e.* solvent mediated, interactions of cations with enzymes. As seen here, the different specific interactions of cations with the solvent impact urease activity with effects comparable to those of anions.

The only exception in the linear B_{JD} trend is the position of Mg^{2+}. This behavior can be explained considering its similarity to Li^+ in terms of their high charge density. Li^+ and Mg^{2+} show also similar ζ-potentials (see Table S4). This behavior is related to their high charge density which reflects their hydration. We recall that the ζ-potential values are derived from the Helmholtz-Smoluchowski equation [58], which accounts only for Coulombic interactions.

3.2. Heavy water

Replacing water with heavy water enables the study of kinetic isotope effects, solvent properties, and hydrogen bonding (HB), that are expected to significantly affect the enzyme activity [59,60]. The reaction rates vary due to the heavier mass of deuterium, highlighting the critical role of hydrogen atoms in these processes. Additionally, the stronger hydrogen bonds formed by heavy water facilitate the investigation of the role of HB in affecting the enzyme structure and active site dynamics [61]. Differences in physicochemical properties also provide insights into solvation and molecular interactions [30,62].

The values of τ and δ in the presence of D_2O are listed in Table S5, and the clock time plots are illustrated in Figure S3 in the Supplementary Materials.

The addition of D_2O causes longer clock times and lower reaction rates (see Fig. 6), with a pretty linear dependence of both τ and δ on the D_2O percentage. The total replacement of H_2O with D_2O is quantitatively comparable to the addition of 50 mM LiCl (see Section 3.1). Considering the reaction rate, even 25 % v/v D_2O causes a rapid decrease in δ compared to water. This suggests that even low amounts of deuterium, and therefore the H-D exchange, induce relevant effects on the enzymatic mechanism.

A reduced reaction rate is expected from the kinetic isotope effect and highlights the importance of water and HB in urease activity. Several hypotheses and considerations can be made:

1. First of all, the reaction starts when urea displaces the three water molecules that close the active site of the enzyme. The findings reported by Marlier *et al.* suggest that the formation of the tetrahedral intermediate, rather than its decomposition into products, represents the rate-limiting step in the hydrolysis process [63]. These water molecules form a tetrahedral template with a Ni^{2+}-bound hydroxyl group, and the interactions are primarily due to hydrogen bonds [64]. Since the urease catalytic mechanism is basically dependent on this water gating cluster (see Figure S2 in Supplementary Materials), we argue that the substitution of hydrogen with deuterium increases the hydrogen bond strength, making it less favorable for the cluster to move away. Additionally, the modified HB distances may distort the optimal conformation for the enzymatic activity, further disturbing the proper interaction with the substrate.
2. The literature is replete with quite different hypotheses for the exact urease reaction mechanism. These mechanisms differ from each other, however many shares common issues [64]. One such point is a Ni^{2+}-coordinated hydroxide that performs a nucleophilic attack on the urea carbonyl C atom, which is a crucial step in the enzymatic hydrolysis [64]. This step can be rate-determining and slow the reaction rate since OD^- bonds are stronger than OH^- bonds, making the nucleophilic attack by OD^- less favorable.
3. Another observation deals with the D/H exchange in urea. Urease releases the first NH_3 from urea, but the second NH_3 results from the spontaneous hydrolysis of the remaining carbamate. However this cannot be the main player, as the hydrolysis rate of carbamate in D_2O and H_2O is known to be similar since 1937 [65]!
4. Moreover, D_2O has different solvation properties. This affects the enzyme hydration (and conformation), that can result in significant effects.

In summary, the observed mechanism likely results from multiple simultaneous effects. We argue that, considering the proposed mechanisms and the enzyme's active site structure, the dominant effect arises from the altered hydrogen bonding of the gating cluster water molecules and the change in the nucleophilic attack rate.

3.3. Degassed solutions

The values of τ and δ in the absence and in the presence of some

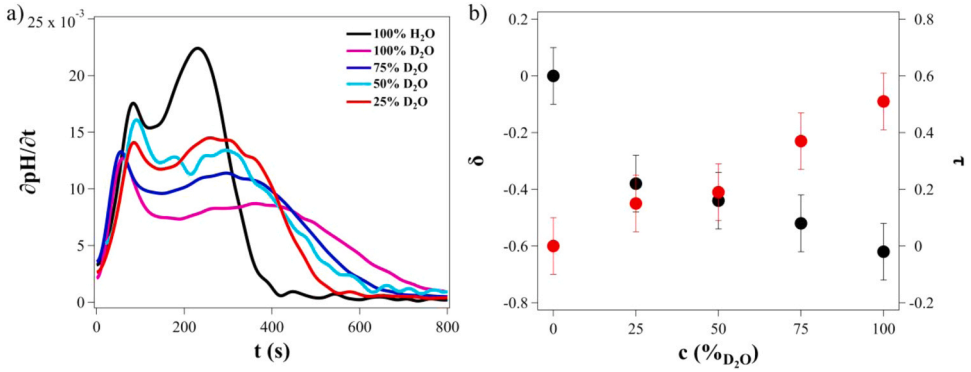

Fig. 6. (a) First derivative ∂pH/∂t *vs.* *t* of pure water, 25 % D_2O, 50 % D_2O, 75 % D_2O and 100 % v/v D_2O. (b) δ (black circles) and τ (red circles) values *vs.* D_2O concentration.

readmitted gases are listed in Table S6, with their relative clock time plots shown in Fig. 7. The degassed solutions show an evident reduced enzymatic activity. This effect on the clock time is comparable to the addition of 0.1 M KCl. The same trend is observed when the degassed solutions were exposed to air for an hour. Instead, after six hours of exposure to air, the reaction rate returned to its original value. This result indicates that the absence of gases has a measurable impact, and that significantly disturbs the properties of water. The perturbation is removed very slowly, as the very slow recovery when the sample is exposed to air indicates.

Readmission of single gases to the degassed solutions shows unique effects depending on the gas. N_2 and Ar caused an acceleration of the urease activity. Interestingly while clock times were longer, the maximum rate of reaction remained equal to that of the blank. On the other hand, the addition of CO_2 greatly reduced it. In fact within the range of investigation, the reaction remained at about pH 5 with a low slope, preventing the calculation of τ and δ. O_2, on the other hand, also caused slower enzymatic activity though to a lesser extent compared to CO_2.

The observed results on the reaction rates can be discussed by invoking different factors.

i. The acceleration of the reaction rate of degassed solutions and those with readmitted N_2 and Ar makes an interesting case. We can explain the behavior by considering the presence of micro- and nanobubbles of air in the solution before degassing. The removal of gases from oil-in-water emulsions has an effect similar to that of adding a surfactant [66]. Moreover, the self-association of bromothymol blue in solution is strongly promoted by the removal of dissolved gasses, again similar to the effects observed with the addition of a surfactant [39]. We argue that these bubbles create a hydrophobic interface on which the enzyme can adsorb [35]. When the dispersion is degassed, these bubbles are depleted, leading to the slowdown of the urea hydrolysis. Conversely, when the degassed solutions are saturated with N_2 or Ar the bubbles regenerate in excess and therefore cause the acceleration of the enzymatic activity. This result is significant for two reasons. First, it suggests that urease activity depends on the presence of nano- and microbubbles in the solvent for proper function. Second, it highlights the unexpected role of inert gases in influencing the enzymatic activity through their mere presence in the solvent.

ii. We recall that hydrophobic cavitation and free radicals affect to some extent the activity of different enzymes [67]. O_2 saturation of degassed solutions produces a significant source of free radicals which are expected to modify the enzyme activity. These radicals can oxidize functional groups such as cysteine residues, aromatic side chains and other reactive moieties critical for maintaining the structural integrity and the conformational stability. Such oxidative modifications may disrupt protein folding, catalytic efficiency, and overall enzyme functionality.

iii. In the case of CO_2 we obtained a deceleration in the enzymatic activity. This result deviates from the literature that instead reports an acceleration [68]. However it is important to recall that our experimental conditions differ from those of the aforementioned study. In fact in the previous work the solution was first saturated with N_2 and then CO_2 was bubbled. Moreover the acidic nature of CO_2 interferes with the pH of the solution that changes during the advancement of the reaction. In a CO_2 saturated solution, the pH increment results in the formation of a quite concentrated CO_2/HCO_3^- buffer (pK_a= 6.35). Therefore, the observed pH *vs.* time curve is influenced by the buffer effect and shows a slower kinetics. This effect becomes evident as the slope of the curve begins to decrease markedly at pH 5. Experiments on the degassed solutions in HEPES buffer at pH 7 confirms this hypothesis as the change in activity is negligible between samples with and without the addition of CO_2 (Figure S4). However, this finding only reflects the effect of CO_2 on the urease activity at this specific pH and does not rule out its potential interactions with the enzyme at other pH values. To this end we recall that the presence of CO_2 is crucial for the urease apoenzyme to bind Ni^{2+} ions and is of paramount importance also for other enzymes in the coordination of metal ions, suggesting a sort of ligand character for CO_2 [69].

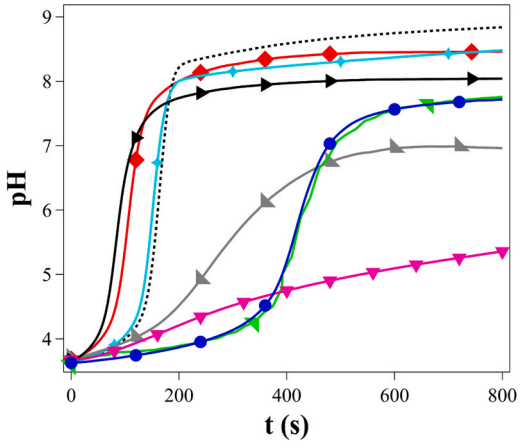

Fig. 7. Plot of pH over time for the blank (dashed line), degassed (•), degassed exposed to air for one hour (◥) and six hours (✦), and solutions with readmitted gases: N_2 (◆), Ar (▸), O_2 (◣) and CO_2 (▾). The curves are the average of multiple measurements.

In conclusion, no matter which mechanism is at work, it seems that the gas nanobubbles in the liquid play a prominent role in driving enzymatic reactions.

4. Conclusions

The kinetics of the urea-urease mechanism was investigated by defining two parameters based on experimental data: i.e. τ, the clock time, and δ, the maximum rate in the pH *vs.* time plot.

The addition of cations at concentrations higher than 10 mM results in the inhibition of the enzymatic reaction, and the specific effect depends on the nature of the ion. The monovalent ions Na^+, K^+, and Cs^+ exhibit similar trends up to high concentrations, above 70 mM. Instead Li^+ induces different effects, similar to those detected in the presence of Mg^{2+}. Interestingly, the δ values for Mg^{2+} and Ba^{2+} overlap, while their τ values are well separated, suggesting that the process is accelerated in the early steps of the hydrolysis.

While the effect of anions on the enzyme activity is well correlated to the interfacial properties of the ions as we reported in a previous work [40], in the case of cations there is no evident correlation between their effect on urease and their interfacial properties. Instead, a linear trend is observed with the cation specific Jones-Dole *B* coefficient with the exception of Mg^{2+}, presumably because of its high charge density and strong hydration properties.

The addition of salts did not seem to modify the secondary structure of urease, as revealed by CD measurement. Instead, the overall effect was an increased population of secondary structures. Additionally, the fluorescence experiments revealed that the ions did not alter the environment of the *Trp* residues, and the only observed effect was dynamic quenching.

These findings overall suggest that cations have an indirect effect on enzyme activity, mediated by their specific interactions with the solvent, which then alters the performance of urease.

The findings obtained in the presence of deuterated water emphasize the significance of the different solvation properties of the solvent and

the pivotal role of hydrogen bonding. We confirm that protons are exceptionally crucial in biological systems, and their substitution with deuterons can lead to substantial consequences.

According to the present study, the presence of gases in the solvent is crucial for the proper functioning of urease. Their effect is discussed in terms of different contributions, and above all on the formation of hydrophobic surfaces due to the presence of nanobubbles dispersed in the reaction medium.

In conclusion, our findings underline the importance of the solvent composition, in terms of added salts, replacement of water with D_2O, and removal of dissolved gases on the enzymatic activity of urease. Understanding intermolecular and interfacial forces is crucial for the advancement of fundamental knowledge, but also for different applications.

Funding sources

P.L.N. ackowledges partial financial support from CSGI (Sesto Fiorentino). F.R. acknowledges financial support under the National Recovery and Resilience Plan (NRRP), Mission 4, Component 2, Investment 1.1, Call for tender No. 104 published on 2.2.2022 by the Italian Ministry of University and Research (MUR), funded by the European Union – NextGenerationEU – Project Title Smart Artificial Cells for Health Applications – CUP B53D23013870006 - Grant Assignment Decree No. 958 adopted on 30/06/2023 by the Italian Ministry of University and Research (MUR), and financial support under the National Recovery and Resilience Plan (NRRP), Mission 4, Component 2, Investment 1.4, funded by the European Union – NextGenerationEU – Project PNRR CN3 "mRNA" CUP B63C22000610006 – Spoke 5.

Supplementary material

Figures of the high-vacuum apparatus, the urease active site, pH versus time plot showing the effect of D_2O at various concentrations, voltage versus time plot of degassed solutions in HEPES at pH 7 and tables presenting the obtained τ, δ and ζ-potential values, deconvolution parameters from fluorescence experiments. (PDF).

CRediT authorship contribution statement

Pierandrea Lo Nostro: Writing – original draft, Supervision, Funding acquisition, Conceptualization. **Federico Rossi:** Writing – original draft, Methodology, Investigation, Conceptualization. **Barry W. Ninham:** Writing – original draft, Conceptualization. **Valentina Romani:** Validation, Investigation, Data curation. **Duccio Tatini:** Writing – original draft, Validation, Methodology, Formal analysis. **Mert Acar:** Writing – original draft, Validation, Investigation, Formal analysis, Data curation, Conceptualization.

Declaration of Competing Interest

The authors declare that they have no known competing financial interests or personal relationships that could have appeared to influence the work reported in this paper.

Appendix A. Supporting information

Supplementary data associated with this article can be found in the online version at doi:10.1016/j.colsurfb.2024.114422.

Data Availability

Data will be made available on request.

References

[1] Y. Miele, S.J. Jones, F. Rossi, P.A. Beales, A.F. Taylor, Collective behavior of urease pH clocks in nano- and microvesicles controlled by fast ammonia transport, J. Phys. Chem. Lett. 13 (2022) 1979–1984, https://doi.org/10.1021/acs.jpclett.2c00069.
[2] G. Hu, J.A. Pojman, S.K. Scott, M.M. Wrobel, A.F. Taylor, Base-catalyzed feedback in the urea−urease reaction, J. Phys. Chem. B 114 (2010) 14059–14063, https://doi.org/10.1021/jp106532d.
[3] I.N. Bubanja, T. Bánsági, A.F. Taylor, Kinetics of the urea–urease clock reaction with urease immobilized in hydrogel beads, React. Kinet. Mech. Catal. 123 (2018) 177–185, https://doi.org/10.1007/s11144-017-1296-6.
[4] E. Jee, T. Bánsági, A.F. Taylor, J.A. Pojman, Temporal control of gelation and polymerization fronts driven by an autocatalytic enzyme reaction, Angew. Chem. Int. Ed. 55 (2016) 2127–2131, https://doi.org/10.1002/anie.201510604.
[5] Y. Miele, Z. Medveczky, G. Holló, B. Tegze, I. Derényi, Z. Hórvölgyi, E. Altamura, I. Lagzi, F. Rossi, Self-division of giant vesicles driven by an internal enzymatic reaction, Chem. Sci. 11 (2020) 3228–3235, https://doi.org/10.1039/C9SC05195C.
[6] B. Krajewska, Ureases I. Functional, catalytic and kinetic properties: a review, J. Mol. Catal. B Enzym. 59 (2009) 9–21, https://doi.org/10.1016/j.molcatb.2009.01.003.
[7] Y. Matsuo, Y. Kido, Y. Yamaoka, Helicobacter pylori outer membrane protein-related pathogenesis, Toxins 9 (2017) 101, https://doi.org/10.3390/toxins9030101.
[8] A. Marghalani, T. Bin Salman, F. Faqeeh, M. Asiri, A. Kabel, Gastric carcinoma: Insights into risk factors, methods of diagnosis, possible lines of management, and the role of primary care, J. Fam. Med. Prim. Care 9 (2020) 2659, https://doi.org/10.4103/jfmpc.jfmpc_527_20.
[9] H. Che, B.C. Buddingh', J.C.M. vanHest, Self-regulated and temporal control of a "breathing" microgel mediated by enzymatic reaction, Angew. Chem. Int. Ed. 56 (2017) 12581–12585, https://doi.org/10.1002/anie.201706716.
[10] N. Gao, M. Li, L. Tian, A.J. Patil, B.V.V.S. Pavan Kumar, S. Mann, Chemical-mediated translocation in protocell-based microactuators, Nat. Chem. 13 (2021) 868–879, https://doi.org/10.1038/s41557-021-00728-9.
[11] T.M. Sutter, M.B. Dickerson, T.S. Creasy, R.S. Justice, Rubber muscle actuation with pressurized CO_2 from enzyme-catalyzed urea hydrolysis, Smart Mater. Struct. 22 (2013) 094022, https://doi.org/10.1088/0964-1726/22/9/094022.
[12] Y. Zhang, P. Li, K. Zhang, X. Wang, Temporary actuation of bilayer polymer hydrogels mediated by the enzymatic reaction, Langmuir 38 (2022) 15433–15441, https://doi.org/10.1021/acs.langmuir.2c02853.
[13] A.M. Adane, S.-Y. Park, Bilayer actuator film for urea biosensing with dual responsiveness: bending actuation and photonic color change, ACS Sens 8 (2023) 2290–2297, https://doi.org/10.1021/acssensors.3c00296.
[14] X. Ma, A. Jannasch, U.-R. Albrecht, K. Hahn, A. Miguel-López, E. Schäffer, S. Sánchez, Enzyme-powered hollow mesoporous janus nanomotors, Nano Lett. 15 (2015) 7043–7050, https://doi.org/10.1021/acs.nanolett.5b03100.
[15] W.-W. Li, Z.-L. Yu, J. Jia, Urease-powered micro/nanomotors: current progress and challenges, J. Pharm. Anal. (2024) 101095, https://doi.org/10.1016/j.jpha.2024.101095.
[16] C. Simó, M. Serra-Casablancas, A.C. Hortelao, V. Di Carlo, S. Guallar-Garrido, S. Plaza-García, R.M. Rabanal, P. Ramos-Cabrer, B. Yagüe, L. Aguado, L. Bardia, S. Tosi, V. Gómez-Vallejo, A. Martín, T. Patiño, E. Julián, J. Colombelli, J. Llop, S. Sánchez, Urease-powered nanobots for radionuclide bladder cancer therapy, Nat. Nanotechnol. 19 (2024) 554–564, https://doi.org/10.1038/s41565-023-01577-y.
[17] H. Choi, S.H. Jeong, T.Y. Kim, J. Yi, S.K. Hahn, Bioinspired urease-powered micromotor as an active oral drug delivery carrier in stomach, Bioact. Mater. 9 (2022) 54–62, https://doi.org/10.1016/j.bioactmat.2021.08.004.
[18] W.T.S. Huck, N. Ivanov, A.I. Slivkov, A urease-based pH photoswitch: a general route to light-to-pH transduction, Angew. Chem. Int. Ed. (2024) e202415614, https://doi.org/10.1002/anie.202415614.
[19] A.Q. Mai, T. Bánsági, A.F. Taylor, J.A. Pojman, Reaction-diffusion hydrogels from urease enzyme particles for patterned coatings, Commun. Chem. 4 (2021) 101, https://doi.org/10.1038/s42004-021-00538-7.
[20] E. Shandilya, A.S. Bains, S. Maiti, Enzyme-mediated temporal control over the conformational disposition of a condensed protein in macromolecular crowded media, J. Phys. Chem. B 127 (2023) 10508–10517, https://doi.org/10.1021/acs.jpcb.3c07074.
[21] R.R. Mahato, Priyanka, E. Shandilya, S. Maiti, Perpetuating enzymatically induced spatiotemporal pH and catalytic heterogeneity of a hydrogel by nanoparticles, Chem. Sci. 13 (2022) 8557–8566, https://doi.org/10.1039/D2SC02317B.
[22] T. Bánsági, A.F. Taylor, Role of differential transport in an oscillatory enzyme reaction, J. Phys. Chem. B 118 (2014) 6092–6097, https://doi.org/10.1021/jp5019795.
[23] A.V. Straube, S. Winkelmann, C. Schütte, F. Höfling, Stochastic pH oscillations in a model of the urea–urease reaction confined to lipid vesicles, J. Phys. Chem. Lett. 12 (2021) 9888–9893, https://doi.org/10.1021/acs.jpclett.1c03016.
[24] Y. Miele, T. Bánsági, A.F. Taylor, F. Rossi, Modelling approach to enzymatic pH oscillators in giant lipid vesicles, in: S. Piotto, F. Rossi, S. Concilio, E. Reverchon, G. Cattaneo (Eds.), Adv. Bionanomaterials (2018) 63–74, https://doi.org/10.1007/978-3-319-62027-5_6. Springer International PublishingCham.
[25] D. Tatini, M. Raudino, M. Ambrosi, E. Carretti, I. Davidovich, Y. Talmon, B. W. Ninham, P. Lo Nostro, Physicochemical characterization of green sodium oleate-based formulations. Part 1. Structure and rheology, J. Colloid Interface Sci. 590 (2021) 238–248, https://doi.org/10.1016/j.jcis.2021.01.040.

[26] P. Lo Nostro, N. Peruzzi, M. Severi, B.W. Ninham, P. Baglioni, Asymmetric partitioning of anions in lysozyme dispersions, J. Am. Chem. Soc. 132 (2010) 6571–6577, https://doi.org/10.1021/ja101603n.
[27] P. Lo Nostro, B.W. Ninham, Hofmeister phenomena: an update on ion specificity in biology, Chem. Rev. 112 (2012) 2286–2322, https://doi.org/10.1021/cr200271j.
[28] B.W. Ninham, Molecular Forces and Self Assembly: In Colloid, Nano Sciences and Biology, Cambridge University Press, Cambridge, 2010.
[29] B.W. Ninham, M.J. Battye, P.N. Bolotskova, R.Yu Gerasimov, V.A. Kozlov, N. F. Bunkin, Nafion: new and old insights into structure and function, Polymers 15 (2023) 2214, https://doi.org/10.3390/polym15092214.
P. Lo Nostro, N. Stubicar, S.-H. Chen, Isotopic effect in phase separation of dioctanoylphosphatidylcholine/water micellar solutions, Langmuir 10 (1994) 1040–1043, https://doi.org/10.1021/la00016a015.
[31] B.W. Ninham, K. Larsson, P. Lo Nostro, Two sides of the coin. Part 2. Colloid and surface science meets real biointerfaces, Colloids Surf. B Biointerfaces 159 (2017) 394–404, https://doi.org/10.1016/j.colsurfb.2017.07.090.
[32] V.S.J. Craig, B.W. Ninham, R.M. Pashley, The effect of electrolytes on bubble coalescence in water, J. Phys. Chem. 97 (1993) 10192–10197, https://doi.org/10.1021/j100141a047.
[33] C.L. Henry, V.S.J. Craig, Inhibition of bubble coalescence by osmolytes: sucrose, other sugars, and urea, Langmuir 25 (2009) 11406–11412, https://doi.org/10.1021/la9015355.
[34] A.W. Nafi, M. Taseidifar, R.M. Pashley, B.W. Ninham, The effect of amino acids on bubble coalescence in aqueous solution, J. Mol. Liq. 369 (2023) 120963, https://doi.org/10.1016/j.molliq.2022.120963.
[35] B.W. Ninham, P. Lo Nostro, Unexpected properties of degassed solutions, J. Phys. Chem. B 124 (2020) 7872–7878, https://doi.org/10.1021/acs.jpcb.0c05001.
[36] A.M. Seltzer, D.P. Nicholson, W.M. Smethie, R.L. Tyne, E. Le Roy, R.H.R. Stanley, M. Stute, P.H. Barry, K. McPaul, P.W. Davidson, B.X. Chang, P.A. Rafter, P. Lethaby, R.J. Johnson, S. Khatiwala, W.J. Jenkins, Dissolved gases in the deep North Atlantic track ocean ventilation processes, Proc. Natl. Acad. Sci. 120 (2023) e2217946120, https://doi.org/10.1073/pnas.2217946120.
[37] M. Lagi, P. Lo Nostro, E. Fratini, B.W. Ninham, P. Baglioni, Insights into Hofmeister mechanisms: anion and degassing effects on the cloud point of dioctanoylphosphatidylcholine/water systems, J. Phys. Chem. B 111 (2007) 589–597, https://doi.org/10.1021/jp065769y.
[38] P. Lo Nostro, L. Giustini, E. Fratini, B.W. Ninham, F. Ridi, P. Baglioni, Threading, growth, and aggregation of pseudopolyrotaxanes, J. Phys. Chem. B 112 (2008) 1071–1081, https://doi.org/10.1021/jp075380q.
[39] D. Tatini, E. Anselmi, G. Cabrucci, M. Acar, B.W. Ninham, P. Lo Nostro, Ionochromism, solvatochromism and effect of dissolved gases on the spectral properties of bromothymol blue, J. Mol. Liq. 365 (2022) 120196, https://doi.org/10.1016/j.molliq.2022.120196.
[40] M. Acar, D. Tatini, M.A. Budroni, B.W. Ninham, M. Rustici, F. Rossi, P. Lo Nostro, Specific anion effects on urease activity: a Hofmeister study, Colloids Surf. B Biointerfaces 236 (2024) 113789, https://doi.org/10.1016/j.colsurfb.2024.113789.
[41] A. Salis, M. Cristina Pinna, D. Bilaničová, M. Monduzzi, P. Lo Nostro, B.W. Ninham, Specific anion effects on glass electrode pH measurements of buffer solutions: bulk and surface phenomena, J. Phys. Chem. B 110 (2006) 2949–2956, https://doi.org/10.1021/jp0546296.
[42] N. Schwierz, D. Horinek, R.R. Netz, Reversed anionic hofmeister series: the interplay of surface charge and surface polarity, Langmuir 26 (2010) 7370–7379, https://doi.org/10.1021/la904397v.
[43] V. Mazzini, V.S.J. Craig, Corrigendum to “Specific-ion Effects in Non-Aqueous Systems, Curr. Opin. Colloid Interface Sci. 38 (82–93) (2018) 214–222, https://doi.org/10.1016/j.cocis.2018.11.001.
[44] V. Mazzini, V.S.J. Craig, Specific-ion effects in non-aqueous systems, Curr. Opin. Colloid Interface Sci. 23 (2016) 82–93, https://doi.org/10.1016/j.cocis.2016.06.009.
[45] B.M. Rode, Y. Suwannachot, The possible role of Cu(II) for the origin of life, Coord. Chem. Rev. 190–192 (1999) 1085–1099, https://doi.org/10.1016/S0010-8545(99)00159-9.
[46] R. Yi, Y. Hongo, I. Yoda, Z.R. Adam, A.C. Fahrenbach, Radiolytic synthesis of cyanogen chloride, cyanamide and simple sugar precursors, ChemistrySelect 3 (2018) 10169–10174, https://doi.org/10.1002/slct.201802242.
[47] D. Tatini, D. Ciardi, C. Sofroniou, B.W. Ninham, P. Lo Nostro, Physicochemical characterization of green sodium oleate-based formulations. Part 2. Effect of anions, J. Colloid Interface Sci. 617 (2022) 399–408, https://doi.org/10.1016/j.jcis.2022.01.135.
[48] E. Jafari Nodoushan, Y.J. Lee, H.-J. Na, B.-H. You, M.-Y. Lee, N. Kim, Effects of NaCl and temperature on rheological characteristics and structures of CTAB/NaSal wormlike micellar solutions, J. Ind. Eng. Chem. 98 (2021) 458–464, https://doi.org/10.1016/j.jiec.2021.03.018.
[49] A. Oren, Life in High-Salinity Environments, in: M.V. Yates, C.H. Nakatsu, R. V. Miller, S.D. Pillai (Eds.), Man. Environ. Microbiol. (2015) 4.3.2-1–4.3.2-13, https://doi.org/10.1128/9781555818821.ch4.3.2. ASM PressWashington, DC, USA.
[50] Y. Marcus, Thermodynamics of solvation of ions. Part 5.—Gibbs free energy of hydration at 298.15 K, J. Chem. Soc. Faraday Trans. 87 (1991) 2995–2999, https://doi.org/10.1039/FT9918702995.
[51] B. Zambelli, F. Musiani, S. Benini, S. Ciurli, Chemistry of Ni^{2+} in urease: sensing, trafficking, and catalysis, Acc. Chem. Res. 44 (2011) 520–530, https://doi.org/10.1021/ar200041k.
[52] W. Yan-Qing, Z. Hong-Mei, Spectral studies on the interaction between Cu2+ and urease, Spectrochim. Acta A. Mol. Biomol. Spectrosc. 96 (2012) 352–357, https://doi.org/10.1016/j.saa.2012.05.014.
[53] J. Zhao, C.-L. Yu, W. Fang, J.-D. Lin, G. Chen, X.-Q. Wang, Spectroscopic and mechanistic analysis of the interaction between Jack bean urease and polypseudorotaxane fabricated with bis-thiolated poly(ethylene glycol) and α-cyclodextrin, Colloids Surf. B Biointerfaces 176 (2019) 276–287, https://doi.org/10.1016/j.colsurfb.2019.01.011.
[54] E.A. Burstein, N.S. Vedenkina, M.N. Ivkova, Fluorescence and the location of tryptophan residues in protein molecules, Photochem. Photobiol. 18 (1973) 263–279, https://doi.org/10.1111/j.1751-1097.1973.tb06422.x.
[55] E.A. Burstein, V.I. Emelyanenko, Log-normal description of fluorescence spectra of organic fluorophores, Photochem. Photobiol. 64 (1996) 316–320, https://doi.org/10.1111/j.1751-1097.1996.tb02464.x.
[56] H.D.B. Jenkins, Y. Marcus, Viscosity B-coefficients of ions in solution, Chem. Rev. 95 (1995) 2695–2724, https://doi.org/10.1021/cr00040a004.
[57] G. Jones, M. Dole, The viscosity of aqueous solutions of strong electrolytes with special reference to barium chloride, J. Am. Chem. Soc. 51 (1929) 2950–2964, https://doi.org/10.1021/ja01385a012.
[58] R.J. Hunter. Foundations of colloid science, 2nd ed, Oxford University Press, Oxford; New York, 2001.
[59] H. Gu, S. Zhang, Advances in kinetic isotope effect measurement techniques for enzyme mechanism study, Molecules 18 (2013) 9278–9292, https://doi.org/10.3390/molecules18089278.
[60] N.V. Yaglova, E.P. Timokhina, S.S. Obernikhin, V.V. Yaglov, Emerging role of deuterium/protium disbalance in cell cycle and apoptosis, Int. J. Mol. Sci. 24 (2023) 3107, https://doi.org/10.3390/ijms24043107.
[61] P. Cioni, G.B. Strambini, Effect of heavy water on protein flexibility, Biophys. J. 82 (2002) 3246–3253, https://doi.org/10.1016/S0006-3495(02)75666-X.
[62] C.V. Krishnan, H.L. Friedman, Solvation enthalpies of various ions in water and heavy water, J. Phys. Chem. 74 (1970) 2356–2362, https://doi.org/10.1021/j100705a020.
[63] J.F. Marlier, L.I. Robins, K.A. Tucker, J. Rawlings, M.A. Anderson, W.W. Cleland, A kinetic and isotope effect investigation of the urease-catalyzed hydrolysis of hydroxyurea, Biochemistry 49 (2010) 8213–8219, https://doi.org/10.1021/bi100890v.
[64] L. Mazzei, F. Musiani, S. Ciurli, The structure-based reaction mechanism of urease, a nickel dependent enzyme: tale of a long debate, JBIC, J. Biol. Inorg. Chem. 25 (2020) 829–845, https://doi.org/10.1007/s00775-020-01808-w.
[65] W. Brandt, Über den Einfluß von schwerem Wasser auf die Harnstoffspaltung durch Urease, Biochem Z. 291 (1937) 9–104.
[66] G.R. Burnett, R. Atkin, S. Hicks, J. Eastoe, Surfactant-free “emulsions” generated by freeze−Thaw, Langmuir 20 (2004) 5673–5678, https://doi.org/10.1021/la049923o.
[67] H.-K. Kim, E. Tuite, B. Nordén, B.W. Ninham, Co-ion dependence of DNA nuclease activity suggests hydrophobic cavitation as a potential source of activation energy, Eur. Phys. J. E 4 (2001) 411–417, https://doi.org/10.1007/s101890170096.
[68] S. Maithani, M. Pal, A. Maity, M. Pradhan, Isotope selective activation: a new insight into the catalytic activity of urease, RSC Adv. 7 (2017) 31372–31376, https://doi.org/10.1039/C7RA05489K.
[69] I.-S. Park, R.P. Hausinger, Requirement of carbon dioxide for in vitro assembly of the urease nickel metallocenter, Science 267 (1995) 1156–1158, https://doi.org/10.1126/science.7855593.